Solid State Electrolyte Sensors for the Determination of Oxygen, Carbon Dioxide, and Total Flow Rates Associated to Respiration in Human Subjects

Edited by: S. Fasoulas

Project participants: R. Baumann[1,2], S. Fasoulas[1], M. Gläser[1], C. Gritzner[1], F. Hammer[2], J. Heisig[1], R. Kahle[1], T. Kirschke[1], T. Schmiel[1], M. Völkel[2]

[1]Institute for Aerospace Engineering, Technische Universität Dresden, 01062 Dresden, Germany
[2]ESCUBE GmbH, Nobelstr. 15, 70569 Stuttgart, Germany

Report No. ILR-RSN P 06-07
13th October 2006
Executive Summary
to the ESTEC Contract No. 15450/01/NL/JS CCN 1, 2, 3

1 Introduction and Background

Since 1993 a considerable amount of research and development has been performed at the Stuttgart University and the TU Dresden on the topic of measuring oxygen partial pressures in various space applications using solid electrolyte gas sensors. These sensors have been applied for example to measure the oxygen amount inside plasma wind tunnels, where modern heat shield materials are tested and qualified as thermal protection shields for re-entry space vehicles. In parallel, different space flight experiments were performed to measure the residual oxygen partial pressure in low earth orbit, which served mainly as precursor experiments for an experiment on-board the International Space Station ("FIPEX on ISS"), which is dedicated to the measurement of the natural and induced environment (atomic / molecular oxygen). This experiment shall be launched to the ISS together with European module "Columbus". Because commercially available sensors did not fulfil the requirements for these space applications, a new sensor development was initiated (Fig. 1).

Very stimulating for the development of the new sensors was also the high interest which simultaneously arose in industry and science for a variety of terrestrial applications, e.g. for environmental and combustion control, medicine and vacuum applications. The reasons were mainly the miniaturised design and other features of the new sensor elements (e.g. capability to detect different gas species, e.g. O_2, H_2, CO, CO_2, etc.). Modern production techniques and innovative materials were then introduced to allow for high quality, reliable, and miniaturised sensor element design (Fig. 2). Another feature, which resulted from the sensor miniaturisation, is the possibility to simultaneously measure other physical properties, e.g. total flow rates. This characteristic made the new sensor elements very attractive for a variety of medical applications on ground and in space.

For example, for many manned space missions, and especially on the ISS, there is a need for a small, lightweight, portable, potentially body-mounted, metabolic gas analyser with which periodic fitness/scientific evaluations on the astronauts could be performed. This device would offer high flexibility to the astronauts, enabling them to conduct experiments at every location on-board the ISS while wearing a mask with the sensor system and performing respiratory experiments. Thus, the device should be capable of being a stand-alone system providing a real-time data display to permit evaluators to monitor data and archiving the metabolic data for post analysis (Fig. 3). Of course, such metabolic gas analyser systems would also have a very high potential for terrestrial applications.

Therefore, the new technological solution was proposed to ESA within the Microgravity Application Promotion (MAP) Programme, AO-99-058, by a group of scientists

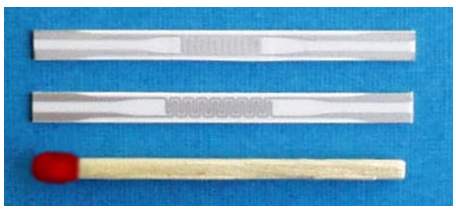

Fig. 1: Sensors used for the space experiment FIPEX on ISS.

Fig. 2: Typical sensor element for terrestrial applications.

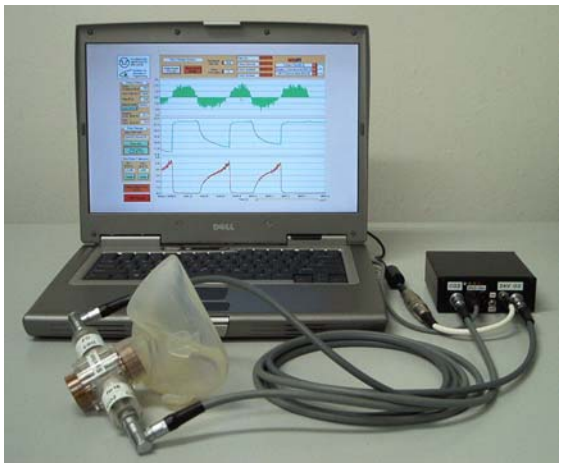

Fig. 3: A complete system for monitoring gas exchange parameters (status January 2005).

and industry. Already at the beginning of the project, the team members identified the following potential advantages of the new system:

- Short response time allowing "breath-to-breath" or even a single breath analysis.
- Measurement in mainstream, capability of measuring O_2, CO_2, and flow rate simultaneously.
- Miniaturised and light-weight design.
- Possibility of mobile/portable use.
- Potential for detecting other gas species.
- Potential for "low-cost" fabrication of sensors.

However, the main objective of this project has been the investigation of the specific scientific and application benefits of the system (including terrestrial applications) and it was not intended to produce a fully functional system. In order to develop such a fully functional system the "Prototype Project" ("Solid State Electrolyte Sensors for the Determination of Oxygen, Carbon Dioxide, and Total Flow Rates Associated to Respiration in Human Subjects" ESA contract No. 15450/01/NL/JS) had been initiated in parallel. The main objectives of this "hardware-oriented", prototype development project have been:

- To advance the flow-sensing capabilities of the solid electrolyte oxygen sensor technology,
- to develop a carbon-dioxide sensor based on the same technology,
- to integrate the technologies into a single, small sensor package, capable of being positioned directly in the inspired/expired flow path of a human subject,
- to perform a preliminary evaluation of such an integrated sensor package,
- to optimise the flow-, O_2- and CO_2-sensor sensitivity, stability and reproducibility,
- to optimise the electronics design, using a smaller amount of components, lower overall power consumption, reduction of housing dimensions, etc.,
- to extend the controller firmware capabilities, including a more complete host-PC interface, a calibration routine, and a flow direction detection,
- to assemble and deliver 3 enhanced demonstration systems, which shall be used / tested within the ESA-MAP-project,
- to redesign the mask adapter with regards to handling, size, and mechanically integration, and
- to perform a first assessment for space application (safety, necessary development efforts, data storage etc.).

Taking into account the planned end-use, the project was aimed at demonstrating that the sensor system provides a performance appropriate for metabolic measurements on human subjects, particularly for manned space missions.

In the following a brief summary of the measurement principles, the design of the sensors and the most interesting results obtained up to now (October 2006) is given.

2 Measurement Principles

2.1 Oxygen Measurement

The working principle of the oxygen and carbon dioxide sensors is based on solid state electrolysis. For the oxygen sensors, yttrium-doped zirconia is used as the electrolyte, which can selectively conduct oxygen ions at higher temperatures (above approx. 450°C). Therefore, the sensor has to be heated up to a constant working temperature. Oxygen concentration is then determined by measuring the current that is conducted through the electrolyte from the cathode to the anode at a constant applied voltage (Fig. 4). If a diffusion barrier limits the oxygen flux from the ambient air to the cathode, the resulting electrical current depends linearly on the ambient oxygen concentration. However, in order to achieve very short response times, the length of the diffusion barrier should be as small as possible. Thus, in the applied planar design, the printed electrolyte itself is one part of the diffusion barrier (Fig. 5) and some additional layers above the electrolyte assist in adjusting the required porosity. Of course, the sensor signal depends also on the working temperature in a relatively complex manner, e.g. by the temperature dependencies of the adsorption/desorption processes on the electrodes, the ionic conductivity of the electrolyte, and by several other occurring physical phenomena that are relevant for the sensor signal.

Thus, the heater design itself is optimised to obtain an uniform temperature distribution on the sensor and to induce only a minimum thermal stress on the sensor. Some of the investigated heater designs are shown in Fig. 6. Of course, in order to minimise heat losses to the surroundings and thus to minimise the overall power demand, the sensor must be insulated adequately (see Fig. 7).

The sensor is manufactured by screen printing and subsequent sintering of several metallic and ceramic layers on a ceramic substrate. This innovative production technique allows for a mass production and miniaturisation of the sensor (Fig. 8). The current sensor size is about 20x3.5x0.5mm. It should be mentioned here that the development of the sensors is an iterative and hardly predictable process, because minimal changes in each layer composition and/or sintering procedure may lead to

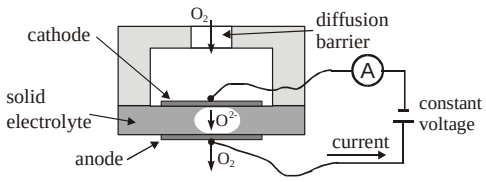

Fig. 4: Working principle of the amperometric oxygen sensor.

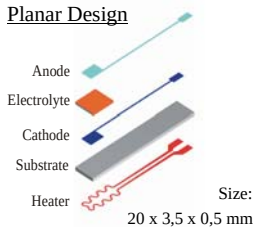

Fig. 5: Main layers of the amperometric oxygen sensor.

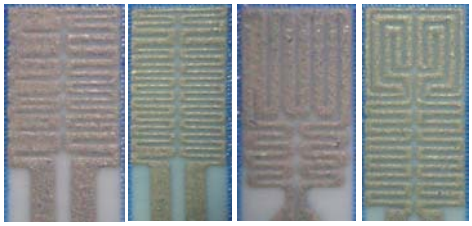

Fig. 6: Some examples of the heater layout.

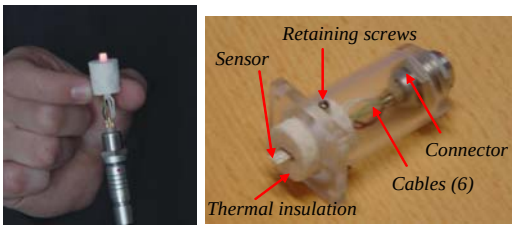

Fig. 7: Miniaturised oxygen sensor (overheated at about 800°C) with insulation and connectors (left) and sensor integrated in the first prototype mask adapter (right).

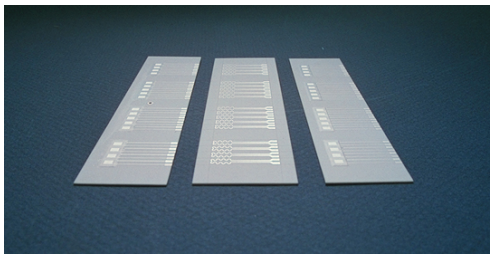

Fig. 8: Substrate with 54 sensors (broken in three parts for illustration).

very different results. Therefore, more than 140 different sensor configurations have been designed, manufactured and analysed. This optimisation process resulted in a remarkable improvement of the sensitivity and stability of the oxygen measurement, leading to an almost ideal characteristic (Figs. 9-11).

Different tests demonstrated the good sensitivity to oxygen and the exceptionally fast response to O_2 changes (e.g. Figs. 12-13). The remaining drift effects are identified to result mainly from inaccuracies in sensor temperature measurement and control, they are not caused by the oxygen measurement itself. Although this influence is relatively low now, a redesign of the electrodes' positions on the sensor will be implemented in the next sensor generation in order to further minimise the influence. Also the temperature control parameters used in the different control algorithms will be further optimised.

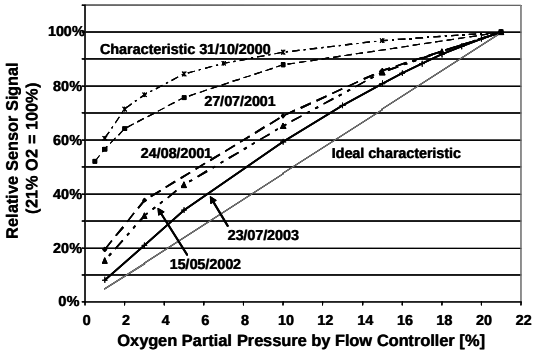

Fig. 9: Characteristics of the different oxygen sensor generations illustrating the improvements in the past (0-21% oxygen). The sensor signals are divided by the sensor signals at 21% O_2.

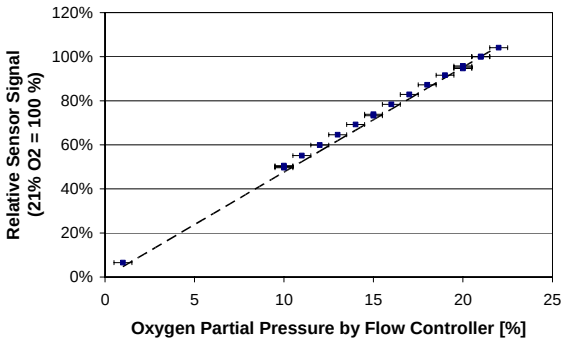

Fig. 10: Characteristic of an oxygen sensor (0-21% oxygen, Jan. 2005). The sensor signal is divided by the sensor signal at 21% O_2. The dashed line marks the ideal characteristic, the error bars indicate the errors in the flow controllers used for calibration.

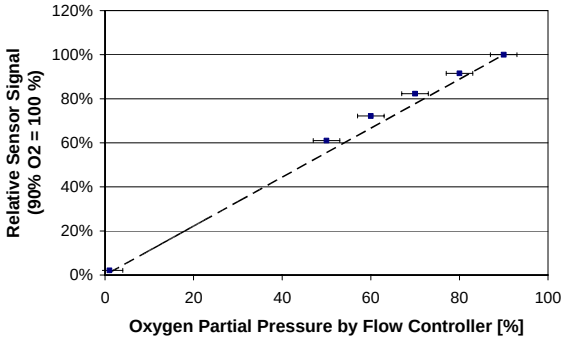

Fig. 11: Characteristic of oxygen sensor (0-100% oxygen, Jan. 2005). The sensor signal is divided by the sensor signal at 90% O_2. The dashed line marks the ideal characteristic, the error bars indicate the errors in the flow controllers used for calibration.

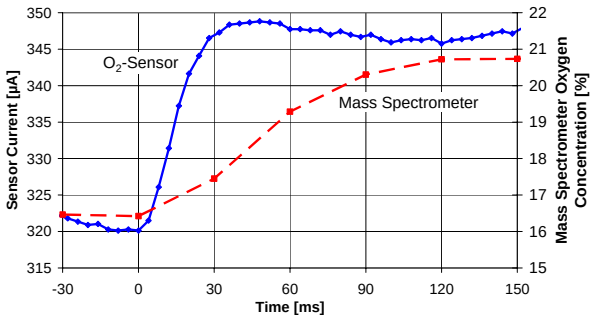

Fig. 12: Evaluation of response times in comparison to a mass spectrometer (test performed at German Sport University, Cologne, with one of the first sensor generations, sensor integrated in mask, all gas exchange effects included).

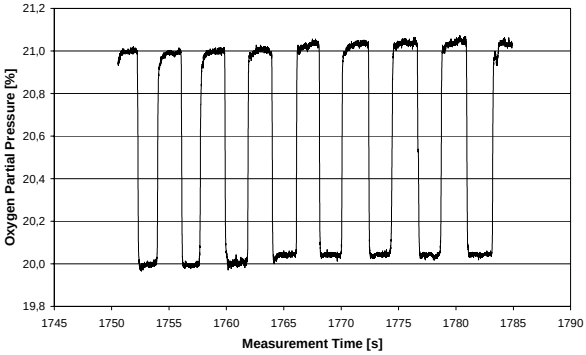

Fig. 13: Measurement by quickly moving sensor into / out of a free stream (free stream: 20 % O2, 1 % CO2, 79% N2).

2.2 Carbon Dioxide Measurement

The development of a respiratory sensor system requires also a fast and reliable measurement of the carbon dioxide concentration. The chosen CO_2 sensors have a similar working principle as the oxygen sensors, their electrolyte material however is based on NASICON (Natrium super ionic conductor). For a simple reproducible serial production, similar to the oxygen sensor, a planar sensor in multi-layer technique is used (Fig. 14). Therefore, different pastes have been developed for the different layers. After the printing process, the pastes have to be sintered at high temperatures. Again, the numerous parameters of these steps have been determined and optimised in various tests.

However, unlike the oxygen measurement, the voltage between the electrodes of the CO_2-sensor depends logarithmically on the partial pressure of CO_2 (Fig. 15) and is independent of the oxygen content. Therefore, in order to obtain accurate measurements, the slope of the characteristic has to be as steep as possible and the main emphasis of the sensor development addresses this issue. Thus, the effect of the error induced by temperature variations of the electrodes, which cause minor voltage changes, gets smaller. On the other hand, the temperature variation of the electrodes depends on the flow rate (i.e. the higher the flow rate the higher the influence).

Generally, the sensor works very well for low CO_2 concentrations (Fig. 16) and/or low flow rates. Because of the logarithmic characteristics, the sensor meets the requirements for higher flow rates regarding precision, resolution, and stability for concentrations up to 2-3% CO_2. For higher concentrations and higher flow rates (above 2 l/s) the characteristics of the sensor has still to be improved. This shall be done by further optimisation of the layer structure, especially by an additional cover layer to prevent the electrodes from a different cool down, and an optimisation of the electrode's orientation on the sensor to minimise temperature differences. In addition, the influence of the flow on cool-down could be minimised by shielding or placing the CO_2-sensor slightly out of the flow.

2.3 Flow Rate Measurement

One basic idea of the solid electrolyte sensor development is to measure both total flow rates and gas concentration simultaneously using a single sensor element with high time resolution.

Therefore, the so-called thin film anemometry was introduced for the total flow rate measurement (Fig. 17). Due to the cooling effect of a gas flow over the hot sensor surface (forced convection), it is necessary to increase the heating power in order to maintain the temperature on a constant level, which is needed for an accurate gas composition measurement anyway. Thus, the sensor electronics control the operating temperature via a resistor heater. Consequently, by measuring the consumed electrical power for keeping a constant sensor temperature, the original cooling fluid flow rate can be determined. However, although the method is well known, a special adaptation to the new sensor system

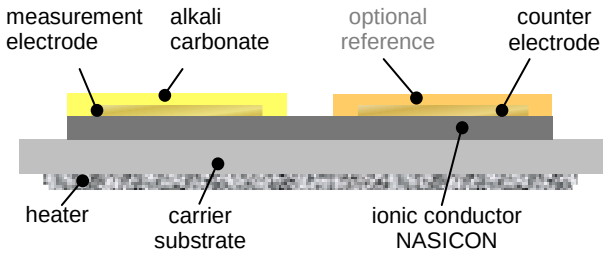

Fig. 14: Planar carbon dioxide sensor design.

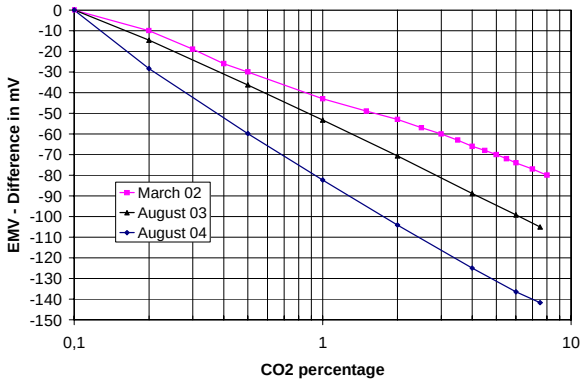

Fig. 15: Evolution of CO_2 sensor characteristics.

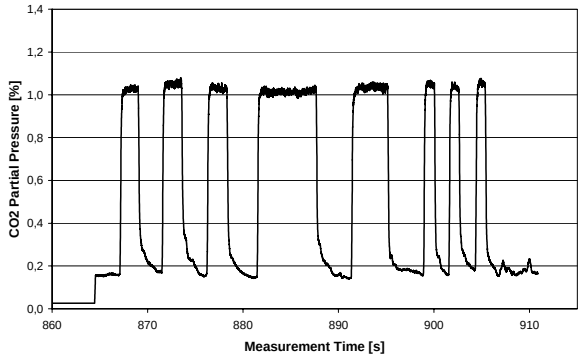

Fig. 16: Measurement by quickly moving sensor into / out of a free stream (free stream: 20 % O_2, 1 % CO_2, 79% N_2).

was incorporated taking into account some basic requirements such as a high time resolution, the relative high thermal capacity of the sensor, and the high temperature level. Therefore, the theoretical understanding of the relevant physical phenomena, as well as the measurement of signals in addition to the power signal, has been necessary to achieve precise flow rate measurements.

For accurate measurements a "smooth" and stable flow pattern has to be established over a high flow rate range. Therefore, several designs of meshes for flow laminarisation as well as different positions and orientations of the sensor within the tube were tested, taking also into account the necessity to minimise the volume within the measurement chamber (Figs. 18-19). However, the most important improvement in flow measurement resulted from the successful implementation of a micro-controller into the sensor control electronics. In combination with various control algorithms the control process showed an almost ideal behaviour and a response time of less than 50 ms was achieved. Fig. 20 shows a typical calibration curve for the flow rate measurement. Figs. 21-22 summarize the comparison of the response time and

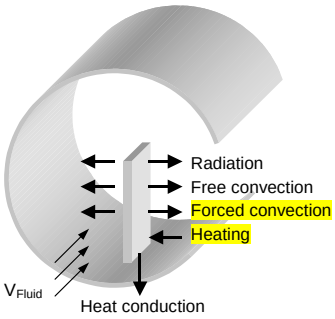

Fig. 17: Measurement principle of thin film anemometry.

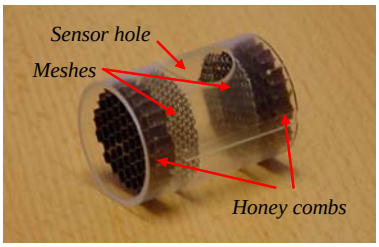

Fig. 18: A prototype of the flow tube with flow pattern improvement, low breathing resistance, and a dead space of about 25 ml.

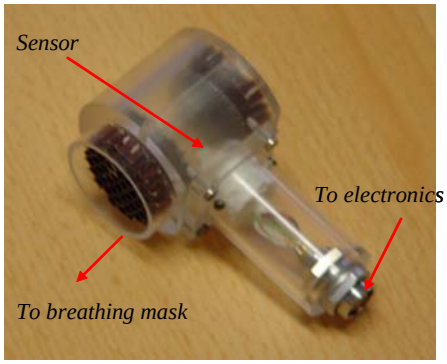

Fig. 19: The assembled prototype sensor system.

accuracy compared to available flow rate measurement devices. In Fig. 21 the results of an early experiment with high flow rates are shown, where the flow direction detection was not incorporated yet. Fig. 22 shows the results at relatively low flow rates, where the information about the flow direction was obtained by the reference flow turbine.

Generally, the flow direction cannot be determined by the necessary heating power only. Therefore, two possibilities were investigated to obtain this information by other means. The first is based on the rapid gas concentration changes, i.e. by measuring the concentration gradients in order to distinguish between inspiration and expiration. However, although this method works well for relatively high flow rates, it introduces a small error due to the dead space of the sensor adapter. Therefore, another solution was tested by measuring the temperature profile on the sensor which depends on the flow direction (Fig. 23). This method works well and it is now integrated in the sensor system.

It should be noted here that the system is currently optimised for relatively high flow rates as associated with the respiration of a human subject. However, the control algorithms and/or the mask diameter can be further optimised in order to allow for a more accurate flow rate measurement at lower flow rates.

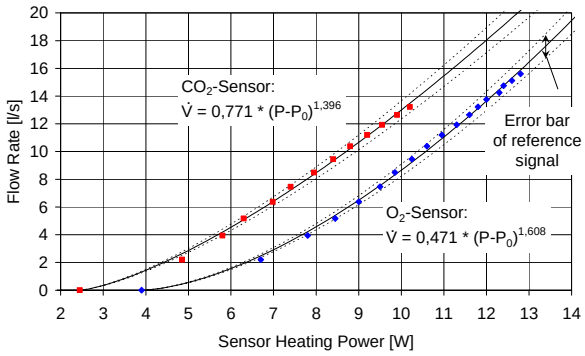

Fig. 20: Typical calibration curve for the flow rate measurement (reference: pressure gauge).

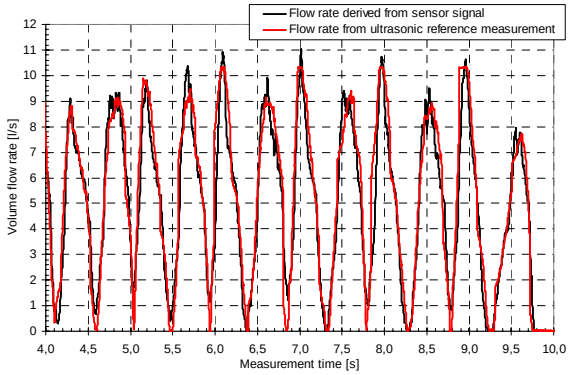

Fig. 21: Comparison of flow rate derived from the solid electrolyte sensor heating power and a reference ultrasonic device.

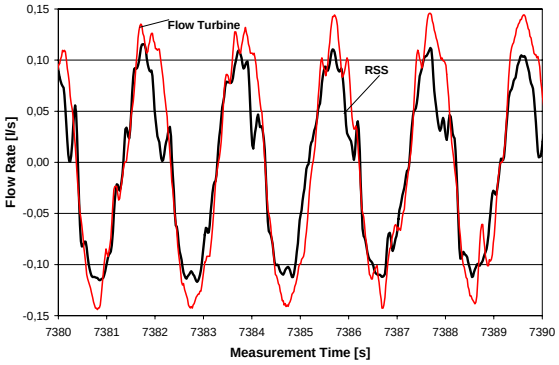

Fig. 22: Comparison of flow rate derived from the solid electrolyte sensor heating power and a reference flow turbine.

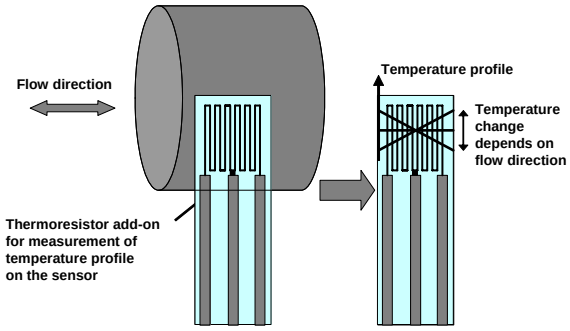

Fig. 23: Basic principle for flow direction detection independent of gas concentration changes.

3 Further Hardware, Software and Investigations

In parallel to the sensor development the digital control electronics (see Fig. 24) and the necessary software have been developed. The data flux in the system is illustrated in Fig. 25, a screen shot of the software in Fig. 26. Also, because of the absolutely new concept of measuring respiratory parameters in-situ, various peripheral hardware, software, and theoretical considerations were developed, improved, and analysed, such as:

- Sensor adapter for the breathing mask (Fig. 19)
- Mask adapters considering flow smoothening and laminarisation aspects (Fig. 18)
- Visualisation software (Fig. 26)

Version (Year)	0.8 (2002)	1.0 (2003/2004)	1.5 (12/2004)
Width	105 mm	105 mm	105 mm
Depth	175 mm	175 mm	118 mm
Height	105 mm	75 mm	39 mm
Volume	1.93 l	1.38 l	0.48 l
Power supply incl.	Yes	No	No
Weight (supply)	1425 g	975 g (600 g)	426 g (600 g)

Fig. 24: The different sensor control electronics developed in the project.

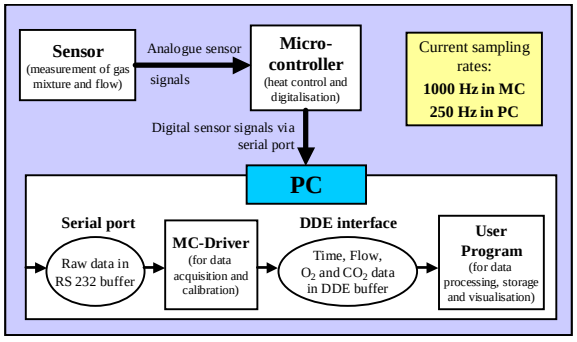

Fig. 25: Scheme of the data flux in the system.

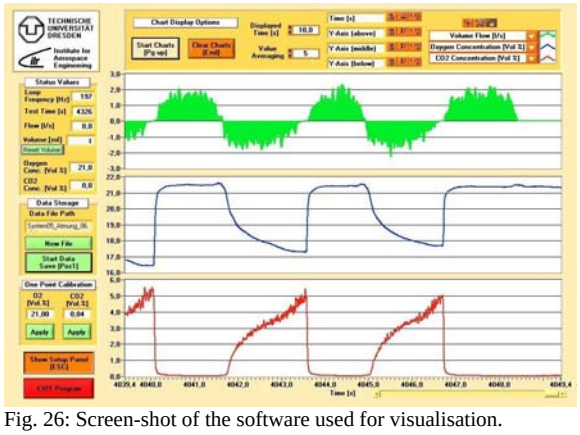

Fig. 26: Screen-shot of the software used for visualisation.

- Application specific software
- Calibration devices
- Simulation devices
- Battery driven system (Fig. 27)
- Alternative data storage (PDA, USB-Memory-Stick see Fig. 27)
- Identification, definition, and conduction of relevant tests.

Furthermore, different design studies have been conducted in order allow for an easier and more reproducible sensor placement in the mask. An example is shown in Fig. 28.

Different validation tests have been conducted in order to analyse the overall sensor system behaviour. Some results were also obtained by testing commercial spiroergometric metabolic carts (e.g. respiratory mass spectrometer, ultrasonic flow meter) and the existing lab system under the aspects of validity, reproducibility, signal stability, and handling in comparison to the targeted applications of the sensor system. Some results are summarized in Figs. 29-32 and in comparison to the requirements in Table 1.

Fig. 27: Electronic unit in current status (PRO1.5) with rechargeable battery pack for an operation time of about 3 hours (left) and communication between the PDA and the RSS-EB (right)

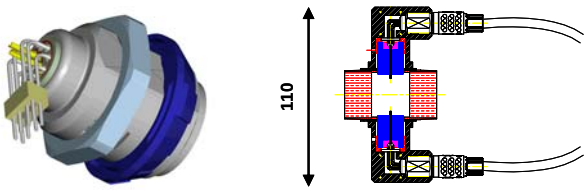

Fig. 28: Design study for a new sensor connector (left) and a complete sensor adapter (right).

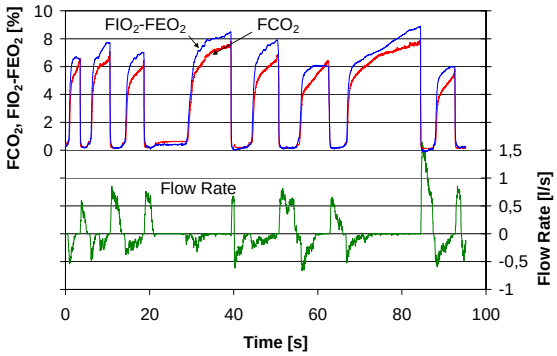

Fig. 29: Test results of the integrated system for low flow rates and moderate breathing frequencies. Inspired oxygen concentration FIO_2 is set to 21%.

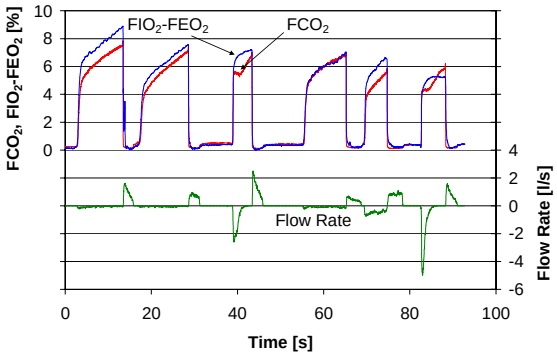

Fig. 30: Test results of the integrated system for moderate flow rates and low breathing frequencies. Inspired oxygen concentration FIO_2 is set to 21%. Results seem reasonable, note however the remaining cross sensitivity of the CO_2-sensor at higher flow rates.

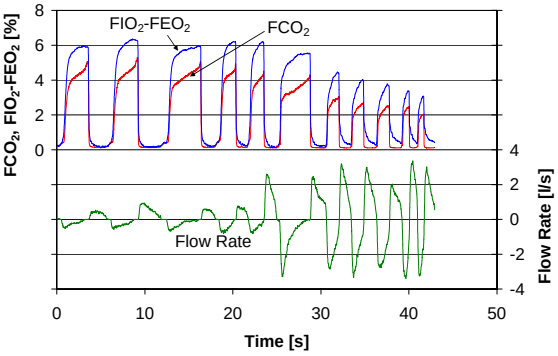

Fig. 31: Test results of the integrated system for moderate flow rates and higher breathing frequencies. Inspired oxygen concentration FIO_2 is set to 21%. Note the cross sensitivity of the CO_2-sensor at higher flow rates.

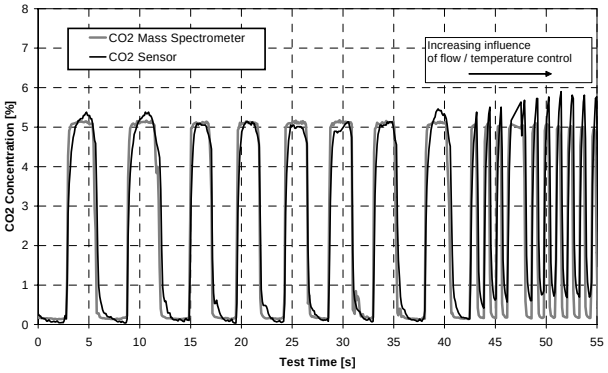

Fig. 32: CO_2 sensor calibration with a gas exchange simulation device at the German Sport University, Cologne; simulation of inhalation: ambient air; simulation of exhalation: 16% O_2, 5% CO_2, 1% Ar, rest N_2; increasing flow rates and breathing frequencies.

Very important for the planned use of the system, especially on space missions, is certainly the overall power demand. Fig. 33 shows the necessary heating power of each sensor and Fig. 34 the power loss in the electronics. In the current status, the overall peak power demand of the system, i.e. for a peak flow rate of approx. 20 l/s, two sensors and electronics version 1.5, may be estimated to be lower than 30 W (without losses of power supply, i.e. AC/DC-converter). The average power demand is about 15 W. However, there are several possibilities to reduce this power demand in the future: The positioning of the sensors can be optimised, smaller sensors can be used, and finally integration of the O_2- and CO_2-sensor on one sensor element. The latter is now foreseen as one of the next development steps as soon as each separate sensor design can be frozen.

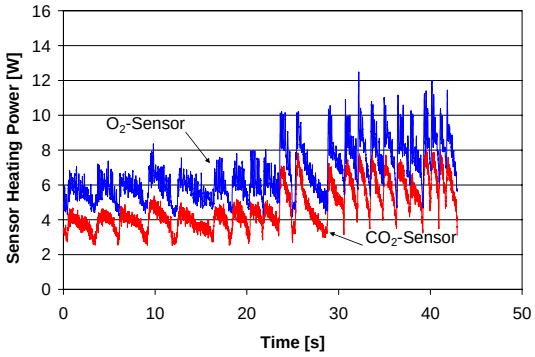

Fig. 33: Heating power required for the sensors (measurement results of this test are shown in Fig. 30). Note that the flow rate is derived in this case from the power consumption of the CO_2-sensor.

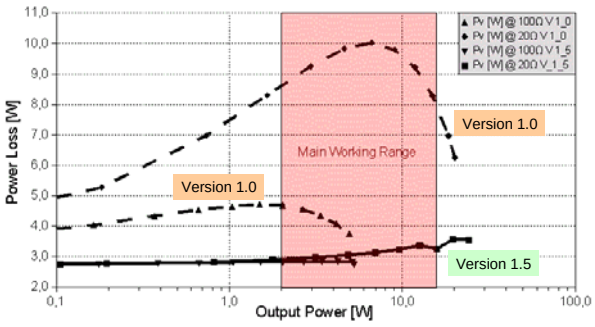

Fig. 34: Power loss in the electronics vs. output power for two different heater resistances. Main issue in the development of version 1.5 was to minimise this power loss.

Fig. 35: The respiratory sensor system – current status. A potential safety risk exists in case of sensor breaking (A: inspiration, B: expiration). Note: Sensor design (especially heater) is optimised to induce minimum thermal stress. After approx. 5 years of sensor testing, having investigated >2.000 sensors, not a single break-up occurred.

Very important cytotoxicity tests concerning the applicability of the sensor system were performed already within the frame of the in parallel ongoing MAP-project. These tests have been performed for the CO_2 and O_2/flow sensors and were conducted according to DIN EN ISO 10993-5, -12, ISO 9363-1, LM SOP 4-06-01. The test results indicated that the sensors do not release substances in cytotoxic concentrations during a 24-hour constant contact period of a 4.5 cm^2 surface area with 1 ml physiological fluid.

Other preliminary investigations were related to safety aspects of the high temperature sensors. A safety risk was identified in the case of sensor destruction as soon as hot fragments are small enough to pass through the surrounding metal mesh. Here, two scenarios were investigated (Fig. 35): First, during inspiration, i.e. fragments move towards test person passing through the mesh, honey comb and biological filter. Here, an estimation of the energy needed to melt the biological filter showed that this energy is higher than the energy content of the largest particle which could pass the laminarisation mesh (size 0.25 mm). Second, also during expiration, the laminarisation mesh provides protection from larger particles with higher overall energy content.

In order to illustrate the broad applicability of the system two other applications are worth to be mentioned here: Centrifuge tests and artificial respiration during an animal surgery.

The centrifuge tests were performed at the DLR Cologne (Fig. 36). The experiment was coordinated by the German sports university Cologne (DSH). The study was aimed to observe the influence of increased gravity to human capabilities and the learning aptitude to the human motor function. A total sum of 30 persons have been tested, 24 students and 6 pilots. The tests were performed under real using conditions, which gave good information about the handling of the prototype. The electronics was specially adapted with an additional event marking and analogue outputs.

The RSS-prototype was used in continuous operation for about 4 hours and more. All of the RSS equipment was used under 3g. Even with the data evaluation still in progress, some first evaluating statements have been given by DSH Cologne:

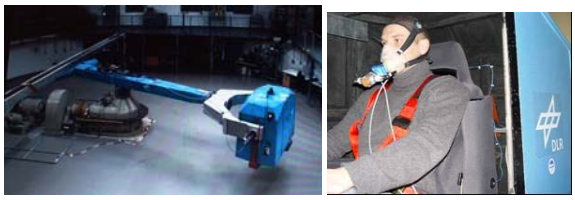

Fig. 36: Centrifuge at DLR Cologne.

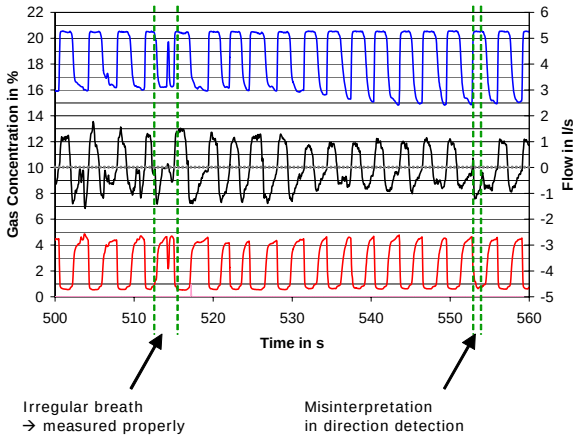

Fig. 37: Exemplary file of obtained data (blue/top curve oxygen concentration, black/mid curve flow rate, and red/bottom curve carbon dioxide concentration.

- Stability of the concentrations displayed by the RSS is very good.
- The inspiratory and end-expiratory values can be used properly (see for example Fig. 37).
- Disturbances in direction detection and offset of switching point did not allow exact volume balance calculations. The concentration independent solution was not implemented yet. The respiratory rate was taken from concentration changes, which could be done properly.

Finally, the RSS PRO 1.5 was tested also under very special conditions. An animal test with a pig was performed while measuring with the RSS in the artificial respiration tube (see Fig. 38). A comparison system for CO_2 measurement as well as for flow and total pressure was integrated into the breathing tube as well. Additionally several medical data for blood concentrations of O_2 and CO_2, heart rate, etc. were recorded.

The tests with the pig represent a good comparison to the physiology of a human subject. However, the size of the pig was about children size (about 25kg). Therefore, the respired volumes are very small. As the RSS-configuration was designed for ergometer tests of adults, the dimensions were too big to achieve optimal results. Nevertheless, the results obtained were extremely informative, revealing results for several breath patterns that have not yet been tested with the RSS prototypes before. A measurement protocol was designed to obtain as much information about the system capabilities under real conditions as possible in only one session. The procedure was defined by the following steps:

1. Variations of inspired oxygen concentration (21%, 40%, 60%, 80%, 100%)
2. Variations in tidal volume (10 ml/kg, 20 ml/kg, 6 ml/kg, 10 ml/kg)
3. Variations in respiratory rate (30 breaths per minute (bpm), 10 bpm, 18 bpm)
4. Variations in artificial respiratory pattern (volume controlled - pressure controlled)
5. Cardiac oscillations
6. Variations of inspired oxygen concentration (100% to 21% to 100%)
7. Simulation of lung illness by lung lavage and optimizing of respiratory pressure
8. Second recruitment (similar to 7.)
9. Cardiac oscillation after lavage

Fig. 38: Pig under anaesthesia with RSS PRO 1.5 and comparison devices.

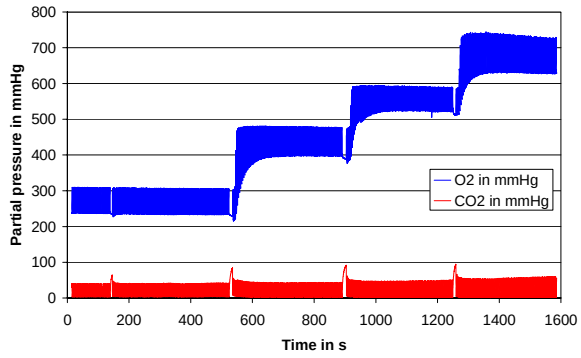

Fig. 39: RSS data of step 1.

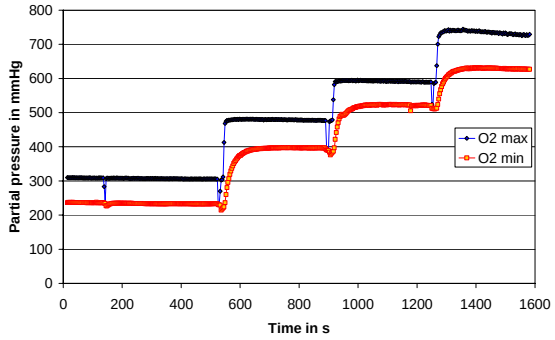

Fig. 40: Maximum inspired and minimum expired oxygen (step 1).

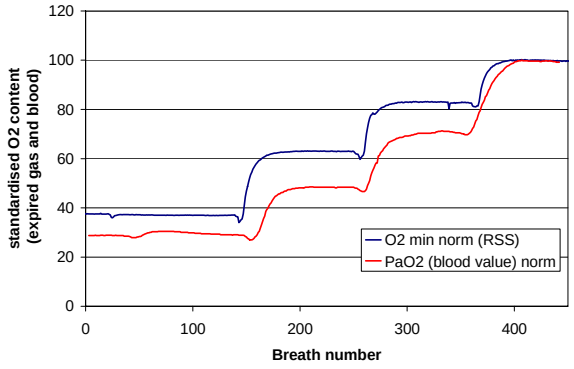

Fig. 41: Comparison of minimum expired oxygen to oxygen content in the blood (step 1, normalised for better comparison).

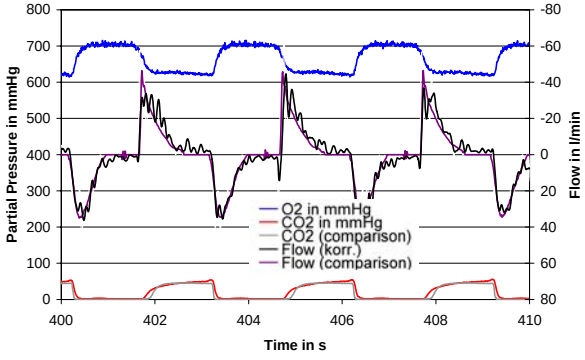

Fig. 42: Zoom of step 3 (medium respiratory rate).

Between every change in conditions a respiratory hold was performed to allow for a better coordination of the different measurement devices.

Some results of this test are shown in the following. The first step could be seen as remarkable. In the overview the complete data for the O_2 and CO_2 measurement were observed (see Figs. 39-40). For each step the partial pressure rises up to a maximum of 750 mmHg (100% at ambient pressure). The expired oxygen level rises slower. Looking at the extreme values, this effect becomes even more clearly. Comparing the minimum level of expired oxygen to the oxygen level in the blood (Fig. 41), a very good analogy was also found. This was postulated by the doctors, but never measured before.

In the test, one important point was to identify the performance of the RSS PRO 1.5 for the single breath analysis, especially for the CO_2 partial pressure measurement. Fig. 42 shows as an example the behaviour of the signals in comparison with a fast CO_2-sensor and a flow sensor. Basically, it seems that the RSS CO_2-sensor matches the comparison device well, but has a slightly longer response time. One main reason is the improvised integration of the sensor in the adapter. One other reason might be that the comparison sensor is influenced/ accelerated mathematically.

Another interesting effect was observed in step 6, when the respiratory oxygen content was switched from 100% to 21% (see Fig. 43-45). As the inspired oxygen is changed rapidly, the expired oxygen level is higher than the inspired one. This was seen until a break-even point is reached and “normal” conditions appear.

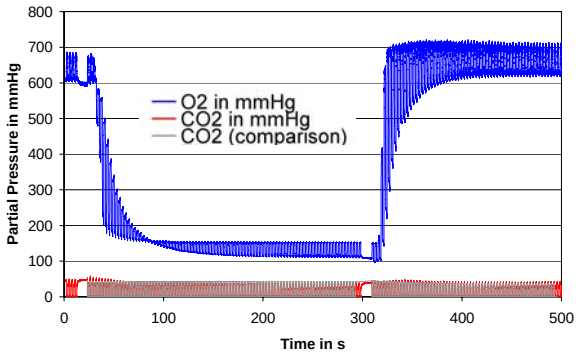

Fig. 43: Overview over step 6 (100% O_2 to 21% to 100%).

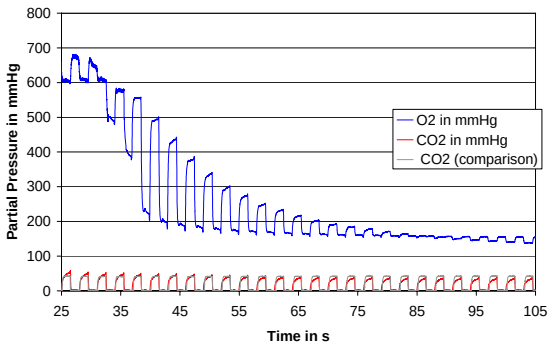

Fig. 44: Step6: Switch from 100% to 21% O_2 inspiration.

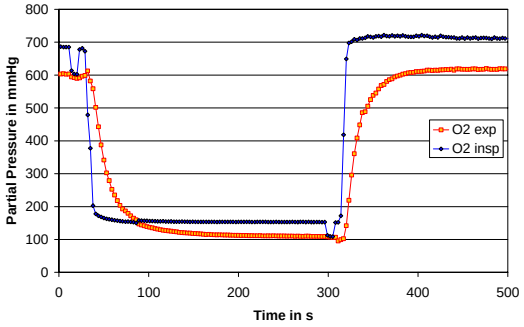

Fig. 45: Step6: End-Inspiratory and end-expiratory oxygen levels based on a breath-to-breath analysis.

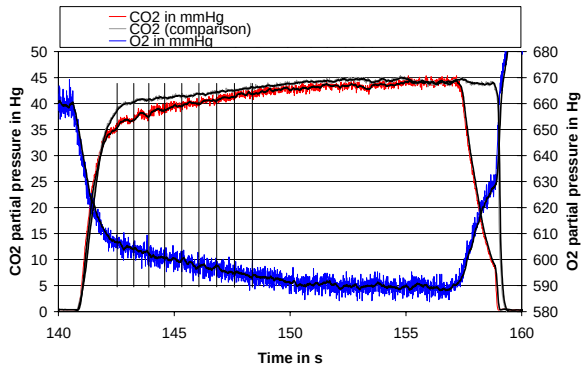

Fig. 45: Observed cardiac oscillations.

Additionally, a good opportunity to observe the RSS sensor response times was given by cardiogenic (or cardiac) oscillations. The heartbeat activates the gas exchange in the lung each beat. This can be observed well in the expired gas flow after holding the breath for a short time. The oscillations can be seen very well in the RSS CO_2-signal (Fig. 46). Normally, the oscillations are very clear in the RSS oxygen signal as well. In this case, the inhaled oxygen content was 100%, the corresponding sensor current switched the current measurement gain in the electronics to the next lower level (1/10), so the signal noise was obviously too high.

4 Summary and Outlook

Within the RSS-project the development of miniaturised sensor systems for respiratory investigations has been certainly advanced. Miniaturised oxygen and carbon dioxide sensors, capable to simultaneously measure also flow rates, have been designed, manufactured, and integrated into a mask for the in-situ measurement of respiratory parameters, and validated in several tests. The sensors seem now applicable for separate measurements of the physical properties in respiratory experiments. Also very important, none of the potential advantages of a fully qualified system had to be withdrawn.

Nevertheless, there are still development and optimisation efforts necessary towards a fully reliable, reproducible, and accurate system. One of the remaining uncertainties is now the simultaneous measurement of higher flow rates with the CO_2 gas sensors. During the development it turned out that the requirements for a constant sensor temperature control, which is needed to minimise cross sensitivities of flow rate to the gas concentration measurement, are much more challenging than originally assumed. However, the development showed also that this issue seems not to be a physical constraint but "only" a matter of control, design of sensor heater and layers, and optimisation of the flow through the mask.

Therefore, the optimisation of the simultaneous measurement should be the main focus in the future in order to improve the overall system performance. In parallel, the system development shall be continuously accompanied by application tests in order to obtain as much information as possible about the operational and scientific limits and constraints, as well as about the potential benefits in comparison to existing systems.

Item	Mass	Remark
Sensor adapter with two sensors (O_2+CO_2)	100 g	See Fig. 19 (shows only one sensor connected), mass requirement can be further reduced
Sensor harness to electronics	354 g	For 2 sensors, not optimised, mass can be reduced further
Mask	137 g	See Fig. 35
Mask fastening net	42 g	See Fig. 35
Biological filter	30 g	See Fig. 35
Electronics	426 g	Version 1.5, Fig. 24
Power supply to electronics	600 g	Standard AC/DC-converter unit for medical applications
RS-232 cable to laptop	122 g	Length of 1.5 m
Total	**1811 g**	

Tab. 2: Overview of overall system mass (status January 2005). Mass demand can and will be further reduced. Thus, the given data should be understood as trend / indicator of the development status.

5 Acknowledgement

The financial support of the development presented in this summary by ESA/ESTEC is gratefully acknowledged. Also, some of the presented qualification results have been obtained with the support of partners. Here, amongst others, the support of Dr. Uwe Hoffmann and Dr. med. Stefan Böhm is gratefully acknowledged.

	Volume flow rate		Oxygen		Carbon dioxide	
	Requirement	**Realised / tested up to now**	Requirement	**Realised / tested up to now**	Requirement	**Realised / tested up to now**
Range	-20 / +20 l/s	-20 / +20 l/s	0…25 %	0…100 %	0…10 %	0…15 %
Response time	< 50 ms	< 50 ms	< 100 ms	< 50 ms	< 100 ms	< 115 ms
Precision	±5% or ±200ml/s, whichever is greater	±100 ml/ s for < 1 l/s ± 3% for > 1 l/s	< ±0.1 % O_2	< ±0.2 % O_2	±0.05 % CO_2	±0.1% for < 4% ± 0.3% for > 4%
Resolution	< 10 ml/s	< 10 ml/s	< 0.05 %	< 0.05 %	< 0.05 %	< 0.05 %
Stability	within precision	within precision	< 0.03 %/h	< 0.2 %/h	< 0.02 %/h	< 0.25 %/h

Tab. 1: Comparison of designated and realised requirements. The experimental results from which the ranges and accuracies were derived, were performed in separate experimental set-ups under laboratory conditions. Thus, the given data should be understood as trend / indicator of the development status.